

Flow parameters derived from impedance pneumography after nonlinear calibration based on neural networks

Marcel Młyńczak¹ and Gerard Cybulski^{1,2}

¹*Institute of Metrology and Biomedical Engineering, Faculty of Mechatronics, Warsaw University of Technology, Boboli 8, 02-525, Warsaw, Poland*

²*Department of Applied Physiology, Mossakowski Medical Research Centre, Polish Academy of Sciences, Pawinskiego 5, 02-106 Warsaw, Poland*
{mlynczak, g.cybulski}@mchtr.pw.edu.pl

Keywords: ambulatory monitoring, impedance pneumography, calibration, neural networks

Abstract: Impedance pneumography (*IP*) is mainly used as a noninvasive method to measure respiratory rate, tidal volume or minute ventilation. It could also register flow-related signals, after differentiation, from spirometry-based forced vital capacity maneuvers or ambulatory-based signals reflecting flow values during natural activity. The aim of this paper is to assess the possibility of improving the accuracy of flow parameters calculated by *IP*, by using nonlinear neural network correction (as opposed to simple linear calibration), and to evaluate the impact of various calibration procedures and neural network configurations. Ten students carried out fixed static breathing sequences, for both calibration and testing. A reference pneumotachometer and the Pneumonitor 2 were used. The validation of calculating peak and mean flow value during each inspiration and expiration was considered. A mean accuracy of 80% was achieved for a separate neural network with two hidden layers with 10 neurons in each layer, trained individually for each subject and body position, using the data from the longest, fixed calibration procedure. Simple linear modeling achieved only 72.5%.

1 INTRODUCTION

1.1 Problem and related works

Respiratory activity appears to be an important factor in physiological analyses, based on measurements carried out both in the laboratory and under ambulatory conditions. Such studies need to extend beyond single spirometry evaluation, gathering the data produced during natural functioning of the subjects (Poupard et al., 2008; Koivumaki et al., 2012).

Impedance pneumography (*IP*) could be used to measure ventilation non-invasively, even for long-term monitoring, impacting the subject's natural activity during registration less than when using face mask (Houtveen et al., 2006; Seppa et al., 2010; Młyńczak et al., 2015b).

Many studies have used impedance pneumography to measure respiratory rate or tidal volume (from which one could estimate minute ventilation) (Houtveen et al., 2006; Seppa et al., 2010; Seppa et al., 2011; Młyńczak et al., 2015b; Młyńczak et al., 2015a; Gracia et al., 2015; Ansari et al., 2016). Those three parameters are the main ones for respiratory

activity under unconstrained conditions, e.g., during sleep (Roebuck et al., 2013; Seppa et al., 2016).

Impedance pneumography provides a volume-related signal. However, it could also be used to measure flow values after differentiation. This could be used to assess spirometry-based parameters, recorded during forced vital capacity (FVC) maneuver (Seppa et al., 2013b), or to enhance the information derived from ambulatory impedance measurement. In the second condition, peak and mean flow during each inspiration and expiration could be calculated.

In a recent work, we assessed the accuracy and reproducibility of linear calibration coefficients on estimation of tidal volume from impedance pneumography (Młyńczak et al., 2015a). Our analysis found greater error in the calculated flow values than in the calculated tidal volumes, compared to reference pneumotachometry (*PNT*). In most cases, the results were underestimated, particularly for greater flow values. This could imply that linear calibration of the impedance signal cannot faithfully reflect changes in flow signal dynamics. Therefore, the assumption made during volume calculations, that the best fitting could be provided by linear regression modeling, ap-

peared to be wrong.

One of the possibilities to deal with this problem are hardware solutions, e.g., applying more sophisticated multifrequency application current signals (multi-sinusoidal or binary one, with specific peaks of frequencies) (Ojarand et al., 2013; Min and Paavle, 2013).

The other possibility may include an implementation of the more advanced signal processing of the *IP* signal, including the way of handling the cardiac component or the calibration strategy (the sequence of differentiation and modeling in relation to the reference data).

Further, nonlinear corrections might be applied in order to handle better signal dynamics. Artificial neural networks have been already used in other scientific disciplines for such issue (Lai et al., 2015; Li et al., 2015). They are also increasingly used in the analysis of respiratory system activity in general (Jafari et al., 2010; Lee et al., 2012; Baemani et al., 2008).

1.2 Objectives

The main objective of this paper is to assess the possibility of improving the accuracy of flow parameters calculated by impedance pneumography, by using nonlinear neural-network correction (as opposed to the simple linear model), based on flow-related signals.

The associated goals are to evaluate, what calibration procedure could provide the best data, leading to the best accuracy in subsequent measurement analysis, and what neural network structure and order of corrections is the most suitable for analysis of the flow parameters.

2 METHODS

2.1 Subjects & Devices

Basic information about the study participants is provided in Table 1. All were generally healthy male students (without any respiratory disease reported) and were informed about the aim of the measurements and gave written consent.

Table 1: Information about the study participants.

	Minimum	Mean	Maximum
Weight [kg]	65.0	77.4	100.0
Height [cm]	171.0	179.3	187.0
BMI	20.75	24.14	33.41
Age	19	23	27

We used our impedance pneumography prototype, Pneumonitor 2, to measure *IP* signals. We used the tetrapolar method, in which two electrodes apply a current signal and the remaining two measure voltage, which is related to the electrical impedance. The configuration proposed by *Seppa et al.* was utilized (Seppa et al., 2013a): receiving electrodes were positioned on the midaxillary line at about 5th-rib level, and application electrodes on the same level on the inner arms.

The Flow Measurement System (by Medikro Oy, Kuopio, Finland) with a Spirometer Unit (M909), a Fleisch-type Heatable Flow Transducer (5530), and a Conical Mouthpiece (M9114), without any resistance, were used as a reference *PNT* device. A 3L syringe was used for daily system calibration to ensure accurate flow values.

The sampling frequency of the reference *PNT* signal was 200Hz , while that of the Pneumonitor 2 is $f_s = 250\text{Hz}$. All signals were transformed (via interpolation) to the latter frequency.

2.2 Protocol & Analysis

The calibration was performed for three body positions (supine, sitting and standing), due to the significant impact of body posture on the calibration coefficients (Młyńczak et al., 2015b). Data for each position were gathered with three different calibration protocols, differing by the duration of registration and breathing regularity:

- free breathing registered for 30 seconds, hereafter called '**Calibration Procedure 1**',
- free breathing recorded for 2 minutes, hereafter called '**Calibration Procedure 2**', and
- fixed breathing, alternately shallow and deep, 4 breaths of each, for each of three frequencies, 6, 10, and 15 breaths per minute (BPM), to evaluate whether signals containing various breathing dynamics (rates and depths) may improve the calibration of flow-related signals, hereafter called '**Calibration Procedure 3**'.

Data for testing were obtained with a fourth procedure, consisting of 6 normal breaths followed by 6 deep breaths (the difference in depth was subjective), for three breathing rates (6, 10 and 15 BPM) and for three body positions (the same as during each calibration procedure). We automatically marked the reference breathing phases (inspiration, expiration, and breathing pause) for each recording using simple amplitude thresholding of the flow-related raw *PNT* signal. We also included in the algorithm heuristics to remove artifacts, very short phases and errors.

Both calibration and test *IP* signals were processed by subtracting the noise component produced by least mean square adaptive filtration from the raw *IP* signal, then smoothing the difference with a 400 ms window. Then, flow-related signals were obtained by second-order differentiation of all *IP* signals. After differentiation, a simple moving-average smoothing method with a 500 ms window was applied, striking a balance between (necessary) removal of the cardiac component and (undesirable) deterioration of the signal dynamics.

The basic calibration could be performed by calculating the single linear coefficient between the *PNT* reference and the processed, flow-related, *IP*-differentiated signal, without needing to take into account the intercept coefficient of the linear model. However, linear calibration for flow signals provides much worse accuracy than for volume signals. Instead, we implemented nonlinear improvement, based on neural networks, using the MATLAB Neural Network Fitting App (described more precisely in the next section) (Mathworks, 2016).

In order to compare flow parameters, absolute and relative errors of maximum flow during inspiration (as a positive value), maximum flow during expiration (as a negative value), and mean flow values during each phase, were calculated. We also provided T-test analysis to evaluate, whether the differences were statistically significant, as well as box, compatibility, and Bland-Altman plots.

Since some artifacts and very quick, unrepresentative breathing phases remained after automatic segmentation, we also provided the analysis after removing 5% outliers, from the inspiration and expiration data, based on the reference *PNT* signal.

All analyses were performed using MATLAB.

2.3 Neural network correction

To fit the neural network, a basic **perceptron architecture (with single-element-vector input, specific numbers of sigmoid hidden layers and neurons in those layers, and a linear output layer)** was applied, taking randomly selected signal samples in each iteration. *IP* was treated as input, and *PNT* as reference/output. During learning procedure the **classic Levenberg-Marquardt back-propagation method** was used, we chose the default division of calibration data into training (70%), validation (15%), and test sets (15%).

We evaluated 13 approaches, listed below. "Individual training" refers to the separate use of the data for each participant, for every calibration procedure and for every body position, as input for a neural net-

work. "Global training" indicates that the signals for all conditions were combined and single neural network was calculated.

1. Only simple linear modeling based on flow-related signals.
2. Neural network with a **single hidden layer with 10 neurons**, trained **individually**.
3. Neural network with a **single hidden layer with 20 neurons**, trained **individually**.
4. Neural network with **two hidden layers of 5 neurons each**, trained **individually**.
5. Neural network with **two hidden layers of 10 neurons each**, trained **individually**.
6. Simple linear modeling and then neural network with a **single hidden layer with 10 neurons**, trained **individually**.
7. Simple linear modeling and then neural network with a **single hidden layer with 20 neurons**, trained **individually**.
8. Simple linear modeling and then neural network with **two hidden layers of 5 neurons each**, trained **individually**.
9. Simple linear modeling and then neural network with **two hidden layers of 10 neurons each**, trained **individually**.
10. Simple linear modeling and then neural network with a **single hidden layer with 10 neurons**, trained **globally**.
11. Simple linear modeling and then neural network with a **single hidden layer with 20 neurons**, trained **globally**.
12. Simple linear modeling and then neural network with **two hidden layers of 5 neurons each**, trained **globally**.
13. Simple linear modeling and then neural network with **two hidden layers of 10 neurons each**, trained **globally**.

Those calibration approaches were performed for signals obtained during each breathing protocol and for all three body positions. In each case, we used the Levenberg-Marquardt back-propagation learning method. The neural networks' architectures were set arbitrarily, in order to evaluate their possible impact on accuracy and learning time.

Due to the fact that the result of the neural network training could be "discontinuous", we performed full accuracy analysis for the best calibration procedure with the addition of moving-average smoothing at the end of the calibration calculations (with an arbitrary window of 200 ms).

As an example, the neural network architecture from the fifth approach is presented in Fig. 1.

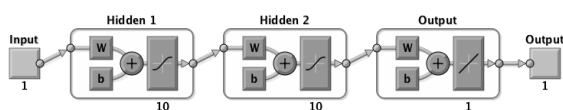


Figure 1: Neural network architecture from the fifth approach (enumerated earlier); abbreviations: W - weight matrix, b - bias vector. (Mathworks, 2016)

3 RESULTS

A sample relationship between the reference *PNT* signal and the flow-related *IP* signal, calculated by the 5th, and 13th calibration approaches, for the second participant in the sitting position, is presented in Fig. 2. An excerpt of those signals (adding the ones for the 1st and 6th calibration approaches), representing two consecutive breaths, is shown in Fig. 3.

Tables 2, 3, and 4 each present the absolute errors, relative errors, and p-values of the maximum and mean flow parameters for Calibration Procedures 1, 2, and 3, respectively (out of the 13 approaches, only the 9 with the best outcomes for each procedure are shown). For the best calibration procedure, we also performed the analysis with smoothed calibration results (with a 200 ms window, hereafter called post-hoc smoothing). The results appear in Table 5.

We did not observe any one participant significantly contributing to the decrease in accuracy. The flow parameters with the smallest overall error were calculated for Calibration Procedure 3, with the 6th calibration approach without any other post-processing, and with the 5th with post-hoc smoothing. It is worth noting that adding the smoothing to the calibration result slightly increased the accuracy, particularly for those calibration approaches in which individually trained neural networks were used.

Generally, combining calculations for peak and mean flow values, Calibration Procedure 3 and the 5th calibration approach seemed best, with 80% mean accuracy, compared to 72.5% for simple linear calibration.

We observed no statistically significant correspondence between flow parameters using the first calibration approach (only simple linear modeling). More complicated calibration procedures yielded lower numbers of neural-network-based approaches in which there was statistically significant correspondence between flow parameters. For the best combination, the differences in peak flow calculations were statistically significant.

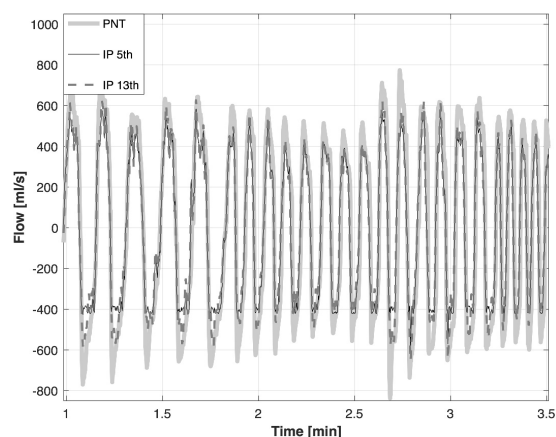


Figure 2: Sample comparison of the 5th, and 13th calibration approach results, calculated from the *IP* signal, in relation to the reference *PNT* signal, for the first participant in a sitting position.

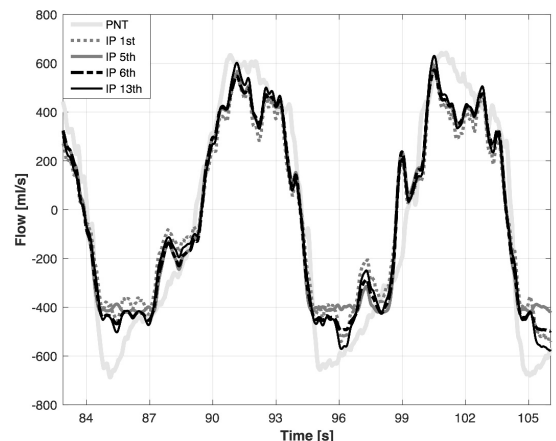


Figure 3: Excerpt of the sample comparison of the 1st, 5th, 6th, and 13th calibration approach results, calculated from the *IP* signal, relative to the reference *PNT* signal, for the first participant, sitting.

Individual neural-network learning was over 14 times faster than global one, comparing 36 seconds to 4 minutes and 12 seconds, on average, respectively. The processing times were measured with the computer processor Intel i5 (1200 MHz), with automatically activated accelerations (up to 2700 MHz).

The box, compatibility, and Bland-Altman plots for the calculated maximum flows for Calibration Procedure 3 and the 6th calibration approach are presented in Fig. 4, 5, and 6, respectively. The same analysis was provided for the 5th calibration approach after applying post-hoc smoothing. The corresponding box, compatibility, and Bland-Altman plots are shown in Fig. 7, 8, and 9, respectively.

Table 2: Comparison of the maximum and mean flow values for the 9 most accurate approaches (considering average error from maximum and mean flow calculations) for **Calibration Procedure 1**; A - absolute error in milliliters per second; R - relative error in percents; p - approximate p-value of paired T test, accurate to the hundredths.

		Calibration Approach								
		1	4	5	6	9	10	11	12	13
Max Flow	A	200.7	246.3	220.9	216.7	233.1	178.9	174.3	175.1	173.6
	R	34.6	35.9	31.3	30.9	33.5	25.5	24.8	24.9	24.8
	p	0.09	< 0.01	< 0.01	< 0.01	< 0.01	< 0.01	< 0.01	< 0.01	< 0.01
Mean Flow	A	187.6	182.1	169.8	173.5	189.6	145.6	145.2	145.8	145.2
	R	43.7	38.2	34.0	34.1	37.9	30.7	30.3	30.4	30.3
	p	0.58	< 0.01	< 0.01	< 0.01	< 0.01	< 0.01	< 0.01	< 0.01	< 0.01

Table 3: Comparison of the maximum and mean flow values for the 9 most accurate approaches (considering average error from maximum and mean flow calculations) for **Calibration Procedure 2**; A - absolute error in milliliters per second; R - relative error in percents; p - approximate p-value of paired T test, accurate to the hundredths.

		Calibration Approach								
		1	2	5	6	9	10	11	12	13
Max Flow	A	142.6	182.4	175.6	197.2	200.1	128.1	136.9	131.5	131.4
	R	26.6	25.4	24.7	28.5	29.3	18.9	19.7	19.3	19.3
	p	0.21	0.85	0.67	0.11	0.18	0.01	< 0.01	< 0.01	0.87
Mean Flow	A	130.8	151.3	147.5	167.7	155.2	118.5	122.3	119.7	119.8
	R	31.6	31.1	29.9	33.3	32.3	26.0	26.7	26.3	26.3
	p	0.92	0.36	0.18	0.01	0.33	0.41	0.07	0.20	0.63

Table 4: Comparison of the maximum and mean flow values for the 9 most accurate approaches (considering average error from maximum and mean flow calculations) for **Calibration Procedure 3**; A - absolute error in milliliters per second; R - relative error in percents; p - approximate p-value of paired T test, accurate to the hundredths.

		Calibration Approach								
		1	2	4	5	6	7	8	11	13
Max Flow	A	144.3	126.8	132.3	118.4	118.5	120.7	118.9	133.0	134.3
	R	28.6	21.1	22.6	20.9	20.8	22.9	20.0	23.9	24.3
	p	0.37	0.04	0.04	0.05	< 0.01	0.01	0.03	0.10	0.26
Mean Flow	A	102.8	89.2	100.3	90.5	87.7	88.6	96.4	84.3	85.1
	R	25.8	22.2	24.2	21.5	21.4	21.6	22.9	20.9	21.3
	p	0.68	0.89	0.93	0.81	0.51	0.95	0.28	0.10	0.18

Table 5: Comparison of the maximum and mean flow values for the 9 most accurate approaches (considering average error from maximum and mean flow calculations) for **Calibration Procedure 3** after **post-hoc smoothing** of the calibration results with a 200 ms window; A - absolute error in milliliters per second; R - relative error in percents; p - approximate p-value of paired T test, accurate to the hundredths.

		Calibration Approach								
		1	2	5	6	7	8	10	11	13
Max Flow	A	144.3	119.0	109.1	109.7	110.0	113.6	130.5	123.7	125.3
	R	28.6	19.5	18.4	19.0	19.3	18.7	22.8	21.6	22.3
	p	0.37	0.04	< 0.01	< 0.01	< 0.01	0.04	< 0.01	0.18	0.36
Mean Flow	A	102.8	90.1	91.4	88.6	89.5	97.4	87.9	85.0	85.9
	R	25.8	23.4	21.6	21.7	22.0	23.2	22.4	21.0	21.4
	p	0.68	0.88	0.80	0.50	0.93	0.28	0.01	0.10	0.18

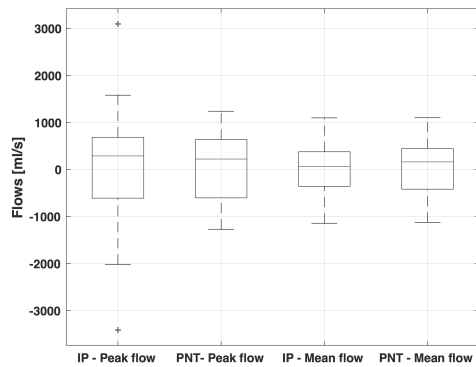


Figure 4: Box-plot comparing the maximum (peak) and mean *IP* and *PNT* flow values and the differences between them, calculated for both inspirations and expirations, for all participants and body positions, for Calibration Procedure 3 and the **6th calibration approach**; positive values correspond to inspiration flows, negative ones - to expiration.

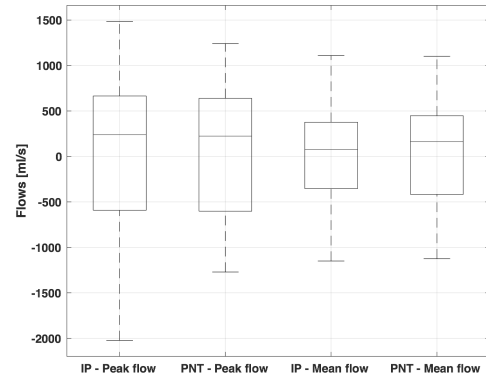


Figure 7: Box-plot comparing the maximum (peak) and mean *IP* and *PNT* flow values and the differences between them, calculated for both inspirations and expirations, for all participants and body positions, for Calibration Procedure 3 and the **5th calibration approach** after post-hoc smoothing; positive values correspond to inspiration flows, negative ones - to expiration.

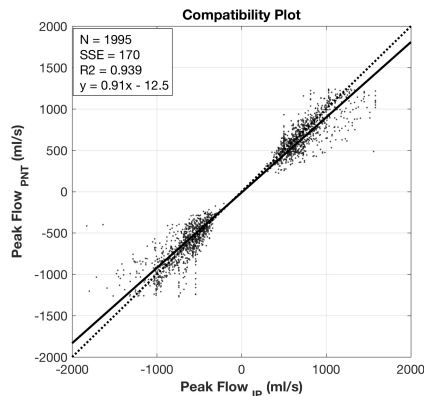


Figure 5: Compatibility plot for maximum flows, calculated for both inspirations and expirations, for all participants and body positions, for Calibration Procedure 3 and the **6th calibration approach**.

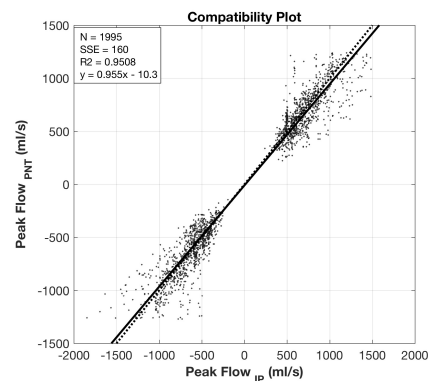


Figure 8: Compatibility plot for maximum flows, calculated for both inspirations and expirations, for all participants and body positions, for Calibration Procedure 3 and the **5th calibration approach** after post-hoc smoothing.

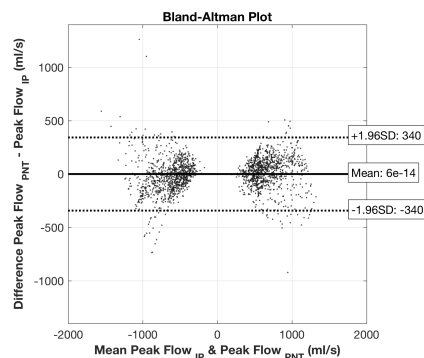


Figure 6: Bland-Altman plot for maximum flows, calculated for both inspirations and expirations, for all participants and body positions, for Calibration Procedure 3 and the **6th calibration approach**.

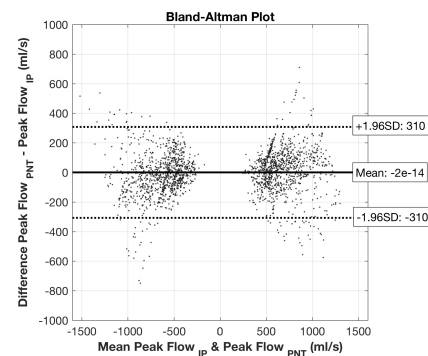


Figure 9: Bland-Altman plot for maximum flows, calculated for both inspirations and expirations, for all participants and body positions, for Calibration Procedure 3 and the **5th calibration approach**, after post-hoc smoothing.

4 DISCUSSION

In general, this paper touches the issue of improving the accuracy of determining the respiratory flow parameters. As the more advanced method, the electrical impedance tomography seems to provide better set of data to estimate ventilation and perfusion as by using "single" signal in impedance pneumography (Leonhardt and Lachmann, 2012).

Nevertheless, in this paper we evaluated the improvement of peak and mean flow estimation accuracy, using differentiated *IP* signal (convenient from the point of view of long-term measurement), resulting from adding neural-network fitting correction or separate modeling. The idea of using the nonlinear correction approach stemmed from the observation that the largest divergence between *IP* and reference signals seemed to be near the peak value.

The verification was performed with different calibration procedures (in order to check which one could provide the best input data leading to the best results during test measurements) and calibration approaches (defining the order of applying linear and neural-network models), with post-hoc smoothing provided for the best calibration procedure (to check the possible impact of appearance of the cardiac component on the calculation).

We used neural networks individually (for specific subject and body position data) or globally (gathering all data), with or without previously applying linear calibration coefficients. The best accuracies were obtained for Calibration Procedure 3, in which breathing rates were fixed and depths of breathing forced. Among them, individually trained neural-network approaches seemed the best in each assessed aspect. The necessity of linear modeling before neural network fitting remains important and in need of evaluation. There is also the question of whether there is an optimal network configuration (number of hidden layers and neurons per layer), or whether it is dependent on the specific subject and measurements being evaluated.

It is worth remembering that the neural-network approach is based on random selection of the input and target data in the learning process. Without setting the seed beforehand, we are unable to obtain the same fit in subsequent repetitions of the training process. Besides, the fitting could be discontinuous (due to the specific data, particularly when there is an artifact in the signals). The subtle post-hoc smoothing was added to deal with that issue.

The individual approach to neural-network fitting reduces learning time. This could be useful with regards to ambulatory monitoring and the prospect

of assessing different network configurations to see which may be best suited to an individual.

The following limitations of this study require mention:

- participants were only 10 males,
- measurements were carried out only under static conditions,
- in ambulatory situations, recordings are longer and more diversified, which may affect overall accuracy,
- there was no distinction of breathing depths, breathing rates, or body positions in the flow accuracy assessment; the results were gathered into the one set, and
- the neural network approach is compared to the use of simple linear modeling calibration coefficient; there is no comparative analysis with another nonlinear methods.

Future plans include:

- assessing the accuracy for models established separately for inspirations and expirations, and for different depth of breathing,
- validating the accuracy in the case of a different order of differentiation and calibration (e.g., linear or nonlinear calibration for volume-related data with differentiation as a final step, performed in order to analyze flow values),
- comparing the results from presented neural-network-based approach with the ones derived from different nonlinear correction algorithm,
- checking the possibility to improve the accuracy by removing the cardiac component adaptively in the way, that the dynamics of the signal changes (particularly for higher flows) is preserved in the most optimal way, and
- evaluating more advanced methods of neural network learning (Monteiro et al., 2016).

5 CONCLUSIONS

The following conclusions may be drawn:

- Non-linear neural-network-based correction of the linear calibration model or a separate neural network fitting model can improve the mean accuracy of peak and mean flow parameters calculated from impedance pneumography signals.
- The longest considered calibration procedure, consisting of fixed breathing with different rates

and depths, allows better coverage of possible flow changes in test signals.

- Neural networks trained individually for every body position of a particular subject seem to provide better results than ones trained with a global set.
- We obtained 80% accuracy with the best combination (separate model based on a neural network with two hidden layers of 10 neurons each, trained individually on the data from 3rd calibration procedure), versus 72.5% for simple linear modeling.

ACKNOWLEDGMENTS

This study was supported by the research programs of institutions the authors are affiliated with.

REFERENCES

- Ansari, S., Ward, K., and Najarian, K. (2016). Motion Artifact Suppression in Impedance Pneumography Signal for Portable Monitoring of Respiration: an Adaptive Approach. *IEEE J. Biomed. Heal. Informatics*, 11(4):1–1.
- Baemani, M. J., Monadjemi, A., and Moallem, P. (2008). Detection of respiratory abnormalities using artificial neural networks. *Journal of Computer Science*, 4(8):663–667.
- Gracia, J., Seppa, V. P., and Viik, J. (2015). Regional impedance pneumography heterogeneity during airway opening pressure chirp oscillations. *Int. J. Bioelectromagn.*, 17(1):42–51.
- Houtveen, J. H., Groot, P. F. C., and De Geus, E. J. C. (2006). Validation of the thoracic impedance derived respiratory signal using multilevel analysis. *Int. J. Psychophysiol.*, 59(2):97–106.
- Jafari, S., Arabalibeik, H., and Agin, K. (2010). Classification of normal and abnormal respiration patterns using flow volume curve and neural network. In *Health Informatics and Bioinformatics (HIBIT), 2010 5th International Symposium On*, pages 110–113. IEEE.
- Koivumaki, T., Vauhkonen, M., Kuikka, J. T., and Hakulinen, M. a. (2012). Bioimpedance-based measurement method for simultaneous acquisition of respiratory and cardiac gating signals. *Physiol. Meas.*, 33(8):1323–1334.
- Lai, C.-L., Lee, J.-S., and Chen, J.-C. (2015). A curve fitting approach using ann for converting ct number to linear attenuation coefficient for ct-based pet attenuation correction. *IEEE Transactions on Nuclear Science*, 62(1):164–170.
- Lee, S. J., Motai, Y., Weiss, E., and Sun, S. S. (2012). Irregular breathing classification from multiple patient datasets using neural networks. *IEEE Transactions on Information Technology in Biomedicine*, 16(6):1253–1264.
- Leonhardt, S. and Lachmann, B. (2012). Electrical impedance tomography: The holy grail of ventilation and perfusion monitoring? *Intensive Care Med.*, 38:1917–1929.
- Li, Y., Pan Fua, Z. L., Lia, X., and Lina, Z. (2015). Biaxial angle sensor calibration method based on artificial neural network. *Chemical Engineering*, 46:361–366.
- Mathworks (2016). Fit Data with a Neural Network. <https://www.mathworks.com/help/nnet/gs/fit-data-with-a-neural-network.html>. [Online; accessed 07-October-2016].
- Min, M. and Paavle, T. (2013). Improved extraction of information in bioimpedance measurements. In *J. Phys. Conf. Ser.*, volume 434, pages 0120291–4.
- Młyńczak, M., Niewiadomski, W., Żyliński, M., and Cybulski, G. (2015a). Assessment of calibration methods on impedance pneumography accuracy. *Biomed. Eng. / Biomed. Tech.*
- Młyńczak, M., Niewiadomski, W., Żyliński, M., and Cybulski, G. (2015b). Verification of the Respiratory Parameters Derived from Impedance Pnumography during Normal and Deep Breathing in Three Body Postures. In *IFMBE Proc.*, volume 45, pages 162–165.
- Monteiro, R. L. S., Carneiro, T. K. G., Fontoura, J. R. A., Da Silva, V. L., Moret, M. A., and De Barros Pereira, H. B. (2016). A model for improving the learning curves of artificial neural networks. *PLoS One*, 11(2).
- Ojarand, J., Annus, P., and Min, M. (2013). Optimisation of multisine waveform for bio-impedance spectroscopy. In *J. Phys. Conf. Ser.*, volume 434, pages 0120301–4.
- Poupard, L., Mathieu, M., Sartène, R., and Goldman, M. (2008). Use of thoracic impedance sensors to screen for sleep-disordered breathing in patients with cardiovascular disease. *Physiol. Meas.*, 29(2):255–267.
- Roebuck, A., Monasterio, V., Geder, E., Osipov, M., Behar, J., Malhotra, A., Penzel, T., and Clifford, G. (2013). A review of signals used in sleep analysis. *Physiological measurement*, 35(1):R1.
- Seppa, V. P., Hyttinen, J., Uitto, M., Chrapek, W., and Viik, J. (2013a). Novel electrode configuration for highly linear impedance pneumography. *Biomed. Eng. / Biomed. Tech.*, 58(1):35–38.
- Seppa, V.-P., Hyttinen, J., and Viik, J. (2011). A method for suppressing cardiogenic oscillations in impedance pneumography. *Physiol. Meas.*, 32(3):337–345.
- Seppa, V.-P., Pelkonen, A. S., Kotaniemi-Syrjanen, A., Makela, M. J., Viik, J., and Malmberg, L. P. (2013b). Tidal breathing flow measurement in awake young children by using impedance pneumography. *J. Appl. Physiol.*, 115(11):1725–31.
- Seppa, V.-P., Pelkonen, A. S., Kotaniemi-Syrjanen, A., Viik, J., Makela, M. J., and Malmberg, L. P. (2016). Tidal flow variability measured by impedance pneumography relates to childhood asthma risk. *Eur. Respir. J.*, pages 1–10.
- Seppa, V.-P., Viik, J., and Hyttinen, J. (2010). Assessment of pulmonary flow using impedance pneumography. *IEEE Trans. Biomed. Eng.*, 57(9):2277–2285.